Available online at www.sciencedirect.com

ScienceDirect

Acta Materialia 89 (2015) 141–152

Acta MATERIALIA

www.elsevier.com/locate/actamat

On the coherency of $Y_2Ti_2O_7$ particles with austenitic matrix of oxide dispersion strengthened steel

Xiaodong Mao,[a] Kyu Hwan Oh,[b] Suk Hoon Kang,[a] Tae Kyu Kim[a] and Jinsung Jang[a,*]

[a]*Nuclear Materials Development Division, Korea Atomic Energy Research Institute, Daedeokdaero 989-111, Yuseong, Daejeon 305-353, Republic of Korea*

[b]*Department of Materials Science and Engineering, Seoul National University, Seoul 151-742, Republic of Korea*

Received 22 July 2014; revised 26 November 2014; accepted 25 January 2015

Abstract—Coherency and orientation relationship of nano-sized $Y_2Ti_2O_7$ particles with an austenitic matrix of oxide dispersion strengthened steel was investigated using selected area diffraction contrast techniques and high resolution transmission electron microscopy. It was revealed that over 95% of the $Y_2Ti_2O_7$ particles (3–10 nm in diameter) are semi-coherent with the austenitic matrix. Perfectly matched planes, which produce no-contrast lines under proper two-beam conditions in transmission electron microscopy (TEM), were obtained across the oxide/matrix interface between parallel planes of $(\bar{2}20)_{Y_2Ti_2O_7}//(200)_{Matrix}$, and $(\bar{3}\bar{3}1)_{Y_2Ti_2O_7}//(0\bar{2}2)_{Matrix}$. A single no-contrast line and multiple no-contrast lines under different active **g**-vectors were observed and discussed. The lattice distortion in the matrix around the $Y_2Ti_2O_7$ particles was determined using the diffraction contrast method under TEM and through X-ray diffraction analyses, which revealed good agreement. A decrease in the inter-planar spacing of up to 7.5% was detected in $(0\bar{2}2)_{Matrix}$ planes owing to the misfit strain at the oxide/matrix interface.

Keywords: Oxide dispersion strengthened steel; Coherency; $Y_2Ti_2O_7$; Orientation relationship; Interface structure

1. Introduction

Oxide dispersion strengthened (ODS) steel has attracted increasing attention as a candidate core structural material for future nuclear reactors [1–5], owing to its high creep strength [6–8] and good irradiation resistance [2,9]. Nano-sized oxide particles dispersed in the matrix act as pinning points for dislocation motion and grain boundary movement, which consequently have significant effects on the microstructure stability and mechanical properties [2,6–8]. Many studies have focused on the characterization of oxide particles in various ODS steels by X-ray diffraction (XRD), high resolution transmission electron microscopy (HRTEM), or atom probe tomography (APT), which demonstrate that the oxide particles are usually non-stoichiometric Ti–Y–O nanoclusters [4,10–12], Y–Al–O complex oxide (such as $YAlO_3$ and $Y_4Al_2O_9$) in Al-alloyed ODS steels [13,14], or Y–Ti–O particles (such as $Y_2Ti_2O_7$ and Y_2TiO_5) in Ti-alloyed ODS steels [11,12,15–17]. These oxide particles are normally smaller than 10 nm in size and show high thermal stability [10–12,17].

As an important fundamental issue, the coherency of the oxide particles with the matrix is closely related to the mechanical properties and microstructure stability of the materials [18–20]. Several studies have focused on the coherency of nano-sized oxide particles with a ferritic matrix in ODS steels. Hirata et al. [11] revealed that non-stoichiometric Y–Ti–O nanoclusters (1–2 nm) are fully coherent with the ferritic matrix, with a NaCl-type crystal structure in 14Cr ferritic ODS steel. Dou et al. [21] showed that fine $YAlO_3$ particles (<4.5 nm) are coherent, and that large $YAlO_3$ particles (4.5–10 nm) are semi-coherent with the matrix in Al-alloyed high-Cr ferritic ODS steel. Recently, Dou et al. reported that δ-phase $Y_4Zr_3O_{12}$ particles improved the coherency with the bcc steel matrix with Zr addition [22], as compared with Al-alloyed high-Cr ferritic ODS steel [21]. Hsiung et al. [14] reported that small $Y_4Al_2O_9$ particles (<10 nm) are coherent or semi-coherent with the ferritic matrix in 16Cr–4.5Al ODS steel. Yttria (Y_2O_3) and complex yttrium titanium oxide particles are found to be partially coherent with the matrix in EUROFER97 ferritic/martensitic ODS steel [23]. Ribis et al. [24,25] demonstrated that $Y_2Ti_2O_7$ particles are coherent and have a cube-on-cube orientation relationship with the ferritic matrix in 14Cr ODS steel.

Austentic ODS steel can have additional advantages in terms of its high corrosion resistance and good microstructural stability. Several studies have focused on the fabrication, microstructure analyses and irradiation tests of austenitic ODS steel [13,26–31]. The orientation

* Corresponding author. Tel.: +82 42 868 2376; fax: +82 42 868 8549; e-mail: jjang@kaeri.re.kr

http://dx.doi.org/10.1016/j.actamat.2015.01.060
1359-6462/

relationship of $Y_2Hf_2O_7$ oxide particles with an Hf-added austenite matrix has been investigated in a recent work [27]. However, there have been few reports concerning the coherency of nano-sized Y–Ti–O particles, which form the major strengthening particle phase in most ODS steels, with the austenitic Fe–Ni–Cr matrix. Since an α to γ phase transformation occurs during mechanical alloying (MA) or subsequent heat treatment, when starting with the element powders (ferritic Fe, Cr and Ni) [13,31], the behaviors of oxide particles in austenitic ODS steel may be different from those in ferritic ODS steel. For instance, a recent study shows that Y_2O_3 particles do not dissolve into the austenitic matrix [13], whereas it was demonstrated that Y_2O_3 particles dissolved into the ferritic matrix and re-precipitated as complex oxide particles [8,10]. This study focuses on the coherency relationship of oxide particles with an austenitic matrix, which may contribute to a further understanding of the pinning effect of oxide particles on the dislocations and grain boundaries within the austenitic matrix, and the formation mechanism of oxide particles in an austenitic Fe–Ni–Cr matrix.

2. Experimental methods

Austenitic ODS steel was fabricated through MA with elemental metal powders (<100 μm) and Y_2O_3 powder (20–50 nm), followed by hot isostatic pressing (HIP), hot rolling, and a solution treatment. The nominal composition of the ODS steel is Fe(bal.)–17Cr–12Ni–2.5Mo–0.3Ti–$0.3Y_2O_3$ in wt.%. An XRD analysis showed that the matrix was fully austenitic. 3 mm diameter disc-type TEM samples were prepared through slicing, mechanical polishing, and twin-jet polishing. Twin-jet polishing was carried out at 25 V and −40 °C in a solution of 5% perchloric acid and 95% methanol. A TEM observation was performed in a JEOL FE2100F high-resolution TEM operated at 200 keV and equipped with an EDS and a double-tilt specimen holder.

The coherency of a large number of oxide particles with the matrix could be judged based on the so-called Ashby–Brown contrast [32]. For an isotropic sphere of a size of r_0 in an infinite isotropic matrix, as schematically shown in Fig. 1, the displacements are radial, and given as a function of the distance r from the center of the particle by

$$\mathbf{R} = \mathbf{C}_\varepsilon r \tag{1}$$

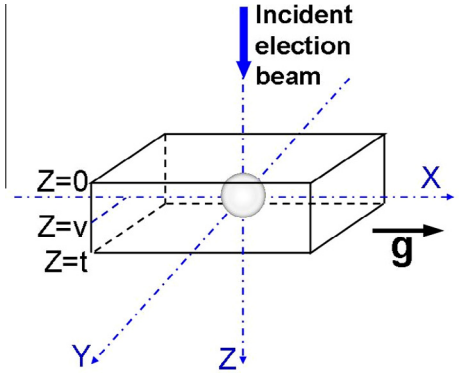

Fig. 1. Coordination system of a particle inside thin film under TEM observation.

when $r < r_0$ and

$$\mathbf{R} = \mathbf{C}_\varepsilon \frac{r_0^3}{r^2} \tag{2}$$

when $r > r_0$, $\mathbf{C}_\varepsilon$ is an expression for the elastic constants, given by

$$\mathbf{C}_\varepsilon = \frac{3K\delta}{3K + 2E(1+v)} \tag{3}$$

K is the bulk modulus of the precipitate; E and v are the Young's modulus and Poisson's ratio, respectively, for the matrix.

To illustrate the formation of a diffraction contrast of nano-sized oxide particles in ODS steel, where a lattice misfit is anisotropic and dependent on the crystallographic orientation of the particle, and interface misfit dislocations are present, the formation of a no-contrast line is introduced based on the study by M.F. Ashby and L.M. Brown in 1963 [32].

Combining (2) with (3), we can obtain

$$\mathbf{R} = \frac{3Kd \times r_0^3}{\left(3K + \frac{2E}{1+v}\right) \times r^2} \tag{4}$$

The important feature is that **R** always has a radial symmetry. Thus, when we consider the Howie–Whelan equation,

$$\mathrm{A_g} = \frac{i\pi}{\xi_\mathrm{g}} \mathrm{A_0} \int_0^t \exp[-2\pi i(s_\mathrm{g} z + \mathbf{g}\cdot\mathbf{R})]\mathbf{dz} \tag{5}$$

If we use the coordinate system shown in Fig. 1, where the positive x-axis is parallel to **g**, $z = v$ at the center of the particle and the thickness of the foil is t, the amplitude diffracted by a column of the matrix around the coherent particle is

$$\mathrm{A_g} = \frac{i\pi}{\xi_\mathbf{g}} \mathrm{A_0} \int_0^t \exp\left[-2\pi i\left(s_\mathrm{g} z + \frac{3K\delta r_0^3 x|\mathbf{g}|}{\left(3K + \frac{2E}{1+v}\right)[x^2 + y^2 + (v-z)^2]^{3/2}}\right)\right] \mathrm{d}z \tag{6}$$

It can be seen from Eq. (6) that, if $x = 0$ (no lattice displacement along the x-axis), then $\mathbf{g}\cdot\mathbf{R} = 0$, and the beam intensity distribution (Howie–Whelan equations) becomes the same with that for a perfect matrix crystal, and a no-contrast line appears on the particle under the active **g**. Therefore, the condition for the appearance of a no-contrast line is that the misfit strain field **R** does not have any component on the lattice plane parallel to the active **g** vector. If a lattice plane of a particle is perfectly matched with a plane of the matrix along the y-axis (perpendicular to the active **g** vector), the lattice distortion along the x-axis will be zero, and a no-contrast line will appear at the position of this pair of perfectly matched planes (as will be shown later in Fig. 5a and c).

In this study bright field images from specific grains were taken. Particles in the grains were analyzed by EDS, and the number of particles was counted. The specimen was tilted by different angles to make sure that all particles were visible and counted. Then, the chosen grain was tilted to a series of two-beam conditions with different **g** vectors, and the number of coherent/semi-coherent particles in the